

Discovering an Image-Adaptive Coordinate System for Photography Processing

Ziteng Cui¹

cui@mi.t.u-tokyo.ac.jp

Lin Gu^{2,1}

lin.gu@riken.jp

Tatsuya Harada^{1,2}

harada@mi.t.u-tokyo.ac.jp

¹ MIL Lab

The University of Tokyo

² RIKEN AIP

Abstract

Curve & Lookup Table (LUT) based methods directly map a pixel to the target output, making them highly efficient tools for real-time photography processing. However, due to extreme memory complexity to learn full RGB space mapping, existing methods either sample a discretized 3D lattice to build a 3D LUT or decompose into three separate curves (1D LUTs) on the RGB channels. Here, we propose a novel algorithm, **IAC**, to learn an image-adaptive Cartesian coordinate system in the RGB color space before performing curve operations. This end-to-end trainable approach enables us to efficiently adjust images with a jointly learned image-adaptive coordinate system and curves. Experimental results demonstrate that this simple strategy achieves state-of-the-art (SOTA) performance in various photography processing tasks, including photo retouching, exposure correction, and white-balance editing, while also maintaining a lightweight design and fast inference speed.

1 Introduction

The Curve & Lookup Table (LUT) serves as an array, replacing runtime computations with a simpler indexing operation. Instead of recalculating results for each operation, precomputed values stored in the table guide input values directly to corresponding outputs. In recent years, deep network based image-adaptive curves (also referred to as 1D LUT) [12, 20, 23, 32, 33, 38] and image-adaptive 3D LUTs [28, 40, 42, 46, 47] have played a crucial role in the image processing era. Compared to methods that use networks for end-to-end mapping, curve & LUT-based methods are highly efficient and can adapt images to arbitrary scale.

Image adaptive curves (IA-curves) adjust R/ G/ B channels individually use 3 curves ($3 \times 1D$ LUT) [23, 32] or use a single curve to uniformly adjust all R, G, and B channels ($1 \times 1D$ LUT) [12, 20]. The advantage of curve-based methods lies in their low computational cost, fast inference time, and ability to specific attribute needs (*i.e.* intensity [12]). However, such operations also pose several challenges because existing curves are primarily built upon the R/ G/ B coordinate axes, which impractical to achieve adjustments for some attributes like hue and saturation [32, 35, 40], moreover, as it shown Fig. 1(a), pixel projections onto R, G,

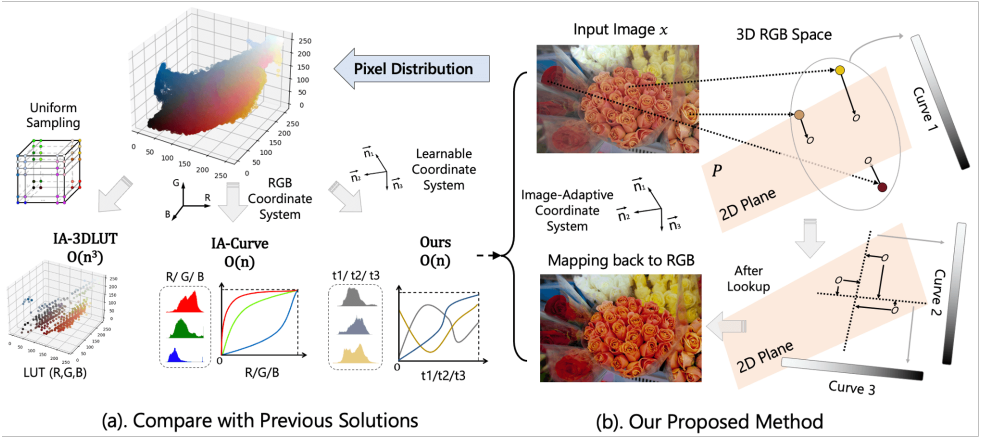


Figure 1: Compare of our **IAC** and previous image-adaptive curve & LUT methods.

and B channels often cluster together, leading to non-uniform sampling and space wastage. Some efforts have been proposed to alleviate this issue, like Kim *et al.* [23] add a pixel-wise local adjustment network after curve adjustment and Moran *et al.* [82] built the curve on multi-colour space, however, these approaches typically add extra computational overhead, also building curves in multiple color spaces increases the network’s learning burden.

Image-adaptive 3D LUTs (IA-3DLUTs) seem to be another solution, which quantize an RGB colour space to grid through uniform sampling (*i.e.* $33 \times 33 \times 33$, $16 \times 16 \times 16$), and perform lookup operations on the sampled grid. Zeng *et al.* [46] and following works [40, 42, 47] use neural networks to learn 3D RGB cube’s grid value, then use trilinear interpolation to predict missing colours in 3D RGB space. Compare to curve, 3D LUT provide more accurate colour adjustments as they operate in 3-dimensional space. However, the spatial domain sampling approach would result in many colors losing their index (ID) in 3D RGB space (see Fig. 1(a)). The subsequent trilinear interpolation relies on CUDA acceleration, which is often memory-intensive and not supported by commonly used frameworks like PyTorch or TFLite on mobile devices [8]. Meanwhile, 3D LUT methods still retain high computational complexity ($O(n^3)$) and also exhibit heavier redundancy in space utilization. For instance, a 33-point image-adaptive 3D LUT typically only utilizes 5.53% of the available space.

After observing the two types of algorithms mentioned above, we thought, why not let the network learn an image-adaptive coordinate space? Where the input image is first projected into its’ preference coordinate system, and then apply curve adjustment in the projected space before transforming back to the RGB space. In this way, we propose **IAC**, which integrate the learning of an image-adaptive coordinate space alongside curve adjustment, allows the network to adapt its coordinate space preferences for each image and task, maximizing targeted considerations while minimizing spatial complexity ($O(n)$). Our solution also requires very little computational cost, and add only a small number of additional coordinate parameters compared to IA-curve methods, which easily enhance the performance and flexibility of the curve. Our contributions can be summarized as follows:

- We first applied the concept of image adaptive coordinate system, which dynamically adjust the coordinate space to better adapt to the image’s own features and variations.
- The advantage of our method lies in its low spatial complexity ($O(n)$). Meanwhile for

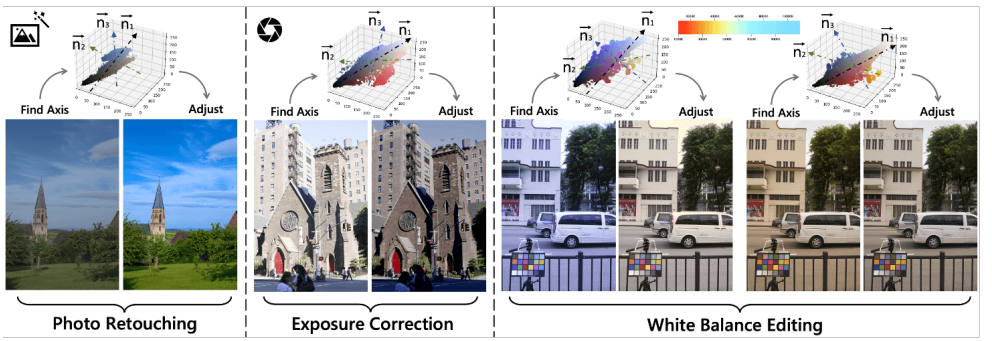


Figure 2: We adopt image-adaptive coordinate system (IAC) for various photography processing tasks, including photo retouching, exposure correction and white balance editing.

network part, our algorithm also maintains a light-weight design ($\sim 39.7K$ parameters), making it feasible to implement on mobile and edge devices.

- Beyond the typical photo retouching tasks, we further validated the potential of our approach in exposure correction and white balance editing tasks. State-of-the-art (SOTA) experimental results demonstrated the effectiveness of our method.

2 Photography Processing

Photography processing aims to handle deviations occurred during the photographs capture stages and deviations introduced in the Image Signal Processor (ISP) stage. Here we primarily focus on three tasks: photo retouching, exposure correction and white balance editing, an overview of these 3 tasks is shown in Fig. 2.

2.1 Photo Retouching

Photo retouching is the process of enhancing an image to improve its appearance, clarity, or the overall quality, which is commonly used in professional photography to create visual pleasant outputs. In earlier decade, people manually adjusted photos or relied on some regression techniques [8] (*i.e.* LASSO Regression [16], Gaussian Process Regression [36]). In the era of deep learning, people achieve end-to-end mapping through neural networks, employing data-driven techniques to automatically train a network capable of adjusting images [8, 7, 12, 14, 15, 22, 23, 24, 31, 32, 37, 39, 40, 42, 43, 44, 46]. Like DeepLPF [31] learns three different types of local parametric filters and regresses the parameters of these spatially localized filters to enhance the image, and DeepUPE [39] introduces intermediate illumination within network to correlate the input with the anticipated enhancement results.

2.2 Exposure Correction

Incorrect exposure times or challenging light conditions can result images with exposure anomalies. Photo exposure correction aims handling both under & over exposure conditions to achieve a more balanced and visually pleasing result.

Traditional exposure correction algorithms [83, 45] prefer to use histogram adjustment to handle exposure error. When it comes to deep learning era, various neural network-based methods [9, 9, 27, 84, 48] have been proposed to address this issue, such as Afifi *et al.* [9] utilized a coarse-to-fine multi scale CNN model, and Cui *et al.* [9] used transformer attention to predict key ISP parameters to correct exposure. Very recently, Nguyen *et al.* [64] designed to use a pseudo ground-truth learning way to achieve unsupervised exposure correction.

2.3 White Balance Editing

White balance (WB) editing aims to correct the acquired sRGB images with wrong white balance setting. This task is more challenging than regular WB correction task which operated on raw-RGB, since illumination estimation is achieved on raw-RGB, once the WB setting is chosen there still remains various other non-linear operation stages in ISP, these operations can increase the complexity of white balance correction. [9, 10].

Afifi *et al.* [9] first introduced this task and proposed a method based on k-nearest neighbor (KNN) to compute a nonlinear colour mapping function for correcting images. After that, various deep learning methods [10, 25, 26] have been introduced in this area, these works aim to accomplish the mapping from error white-balance (WB) images to correct WB images through an end-to-end network based approach.

In this paper, we will evaluate our method on the aforementioned three tasks to confirm the effectiveness of our image-adaptive coordinate system in diverse scenarios. Experimental results demonstrate that our approach achieves state-of-the-art (SOTA) performance across all three tasks while maintaining time and parameter efficiency.

3 Image-Adaptive Coordinate System

An overview of IAC algorithm is shown in Fig 1(b). Given an image $x(r, g, b)$ in the RGB colour space $\mathbb{I}(R, G, B)$, our goal is to learn x 's most suitable coordinate projection vectors $\{\vec{n}_1, \vec{n}_2, \vec{n}_3\}$, image x would be mapped along $\{\vec{n}_1, \vec{n}_2, \vec{n}_3\}$ to projected in new coordinate system, then adjusted with 3 curves on new coordinate system. Both of the projection vector $\{\vec{n}_1, \vec{n}_2, \vec{n}_3\}$ and curves $\{curve_1, curve_2, curve_3\}$ are learned from network \mathbb{N} .

3.1 Methodology

Image-adaptive coordinate system's vectors \vec{n}_1 , \vec{n}_2 and \vec{n}_3 are three 3-dimensional linearly independent vectors, which form a 3×3 invertible matrix:

$$[\vec{n}_1, \vec{n}_2, \vec{n}_3] = \begin{bmatrix} a_1 & a_2 & a_3 \\ b_1 & b_2 & b_3 \\ c_1 & c_2 & c_3 \end{bmatrix}, \quad (1)$$

where the RGB colour space could be seem as a special case when $[\vec{n}_1, \vec{n}_2, \vec{n}_3]$ is an identity matrix. Input image $x(r, g, b) \in (H, W, 3)$ would multiply to matrix $[\vec{n}_1, \vec{n}_2, \vec{n}_3]$ and project onto the new coordinates space (depicted as (a) in Fig.3):

$$\begin{aligned}
F(x) &= x \cdot [\vec{n}_1, \vec{n}_2, \vec{n}_3] = [x \cdot \vec{n}_1, x \cdot \vec{n}_2, x \cdot \vec{n}_3] \\
&= [x(r), x(g), x(b)] \cdot \begin{bmatrix} a_1 & a_2 & a_3 \\ b_1 & b_2 & b_3 \\ c_1 & c_2 & c_3 \end{bmatrix} = [t_1, t_2, t_3]
\end{aligned} \tag{2}$$

where :

$$t_i = x(r) \cdot a_i + x(g) \cdot b_i + x(b) \cdot c_i \quad i \in (1, 2, 3).$$

Following Eq.2, the image $x(r, g, b)$ would be projected with the matrix $[\vec{n}_1, \vec{n}_2, \vec{n}_3]$ to $F(x)$. The projection results are represented as $F(x)(t_1, t_2, t_3)$, where t_1, t_2, t_3 are the projected values in the new coordinate space. Then, adaptive curves $curve_1, curve_2, curve_3$ would be built on the t_1, t_2, t_3 channels to adjust the value of $F(x)$ (depicted as (b) in Fig.3). Here, we normalize the range of t_1, t_2, t_3 between 0 and 1. Meanwhile, the curves also range from 0 to 1, and for each curve, we designed it as 200 dimensions¹. Then we adjust the pixel value through curves $\{curve_1, curve_2, curve_3\}$:

$$t'_i = curve_i(t_i) \quad i \in (1, 2, 3), \tag{3}$$

values in $F(x)(t_1, t_2, t_3)$ after curve mapping adjustment would be $L(F(x))(t'_1, t'_2, t'_3)$, here we first perform a denormalization to recover $L(F(x))$'s normalized value, then multiply to $[\vec{n}_1, \vec{n}_2, \vec{n}_3]$'s inverse matrix to map $L(F(x))$ back to RGB colour space and get final results (depicted as (c) in Fig.3):

$$F^{-1}(L(F(x))) = L(F(x)) \cdot [\vec{n}_1, \vec{n}_2, \vec{n}_3]^{-1}. \tag{4}$$

We will initialize the matrix $[\vec{n}_1, \vec{n}_2, \vec{n}_3]$ as an invertible matrix, and in order for the matrix $[\vec{n}_1, \vec{n}_2, \vec{n}_3]$ to be invertible during learning stage, if the rank of the learned matrix $[\vec{n}_1, \vec{n}_2, \vec{n}_3]$ less than 3, we will add a set of small random numbers to help it recover to rank 3.

Afterwards, we will compute loss function (*i.e.* L1 loss) between $F^{-1}(L(F(x)))$ and the ground truth x_{gt} to optimize network \mathbb{N} , then help us find the most suitable image-adaptive coordinate projection vectors $[\vec{n}_1, \vec{n}_2, \vec{n}_3]$ and curves.

3.2 Network Design

In this section we introduce **IAC**'s network design, network \mathbb{N} is responsible to predict image-adaptive coordinate system $\{\vec{n}_1, \vec{n}_2, \vec{n}_3\}$ and curves $\{curve_1, curve_2, curve_3\}$, additionally **IAC** is a general approach that could also be implemented in other framework.

As shown it in Fig. 3, input image x first passes through 3 down-sampling blocks, each down-sampling block consists of a down-sampling ($\downarrow 2$) 3×3 convolution, batch normalization and a GELU activation [14]. After down-sampling process, we designed a parallel generator to predict image adaptive coordinate and curves. The parallel generator comprises three parallel branches: $\mathbb{G}_1, \mathbb{G}_2, \mathbb{G}_3$, each branch consists of several ConvNext [29] blocks, where we set the block number to 3 in our experiments, for each ConvNext [29] block, it consists of a 7×7 depth-wise convolution, two 1×1 convolutions, layer normalization (LN), and GELU activation [14], channel number of convolution blocks is set to 32, also the entire structure is linked by a residual operation. The large convolution design allows **IAC** to more

¹For more details, please refer to our supplementary part.

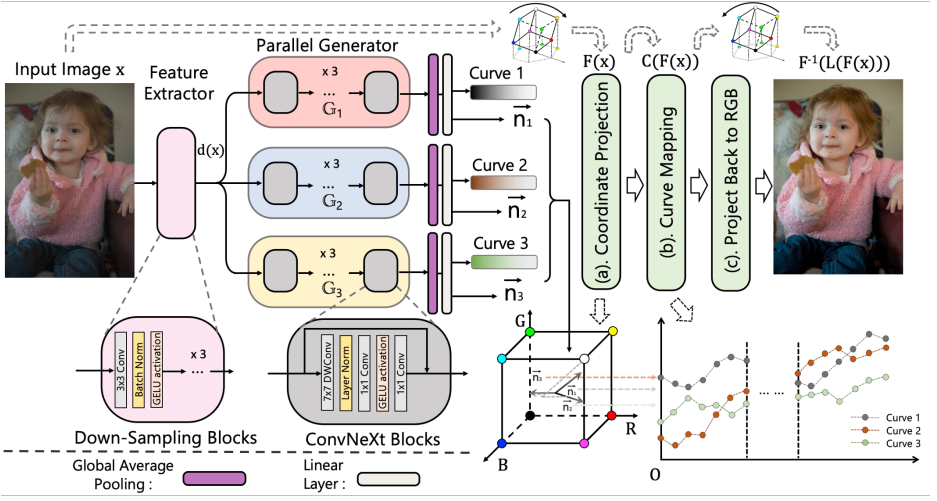


Figure 3: An overview of IAC’s network architecture, image x would pass by network \mathbb{N} to generate coordinate system vectors $\{\vec{n}_1, \vec{n}_2, \vec{n}_3\}$ and curves $\{curve_1, curve_2, curve_3\}$.

effectively extract image features, which also enabling us to better acquire the global-wise image information.

Among three parallel branches: $\mathbb{G}_1, \mathbb{G}_2, \mathbb{G}_3$, branch \mathbb{G}_1 is responsible to predict vector \vec{n}_1 and $curve_1$, feature pass by \mathbb{G}_1 ’s ConvNext blocks would go through a global average pooling layer and linear layer to predict $\vec{n}_1 = [a_1, b_1, c_1]$ and $curve_1$. Similarity, branch \mathbb{G}_2 is responsible to predict \vec{n}_2 and $curve_2$ and branch \mathbb{G}_3 is responsible to predict \vec{n}_3 and $curve_3$. After that the predicted vectors and curves would process input image x , as we mentioned in Sec. 3.1. Please refer to our supplementary for more structure details.

4 Experiments

In this section, we selected 3 tasks to validate the effectiveness of our image-adaptive coordinate (IAC) method, including (a). photo retouching, (b). exposure correction and (c) white balance editing. We would detailed introduce the experiments as follow ²:

4.1 Photo Retouching Experiments

We conclude photo retouching experiments on MIT-Adobe FiveK [5] dataset, MIT-Adobe FiveK dataset consists of 5000 images, each meticulously adjusted by five experts (A/B/C/D/E). Following previous works [81, 89, 46], we employ images adjusted by expert C as the ground truth references. And compare our methods with various SOTA photo retouching methods include DeepUPE [89], DPE [7], HDRNet [12], DeepLPF [12], DPED [19], CURL [82], 3D LUT [46] and AdaInt [42], it worth to note that 3D LUT and AdaInt are 2 image-adaptive 3D LUT methods which must rely CUDA to acceleration. Comparison results are shown in Table. 1, our IAC approach could gain best image quality performance (PSNR, SSIM) among non-CUDA methods, meanwhile keep an extremely lightweight design (39.7K parameters)

²For more experimental details and training setting, please refer to our supplementary part.



Figure 4: Visualization of photo retouching results on MIT-Adobe FiveK dataset [5].

Table 1: Experimental results on MIT-Adobe FiveK [5] dataset, we compare PSNR \uparrow , SSIM \uparrow , parameter number (# Para) \downarrow and inference time \downarrow . Here best results are marked as red and best results without CUDA operation are marked as blue.

	DeepUPE	DPE	HDRNet	DeepLRF	DPED	3D LUT	AdaInt	CURL	IAC (Ours)
PSNR	21.88	23.75	24.66	24.73	21.76	25.29	25.49	24.04	25.02
SSIM	0.853	0.828	0.875	0.916	0.871	0.922	0.926	0.900	0.902
Need CUDA ?	×	×	×	×	×	✓	✓	×	×
# Para	927.1K	3.4M	483.1K	1.7M	-	593.7K	619.7K	1.4M	39.7K
Inference Time	0.628s	0.534s	0.673s	1.287s	-	0.012s	0.018s	0.834s	0.014s

and fast inference time. Some visualization examples are shown in Fig. 4, our **IAC** could produces ideal colour restoration results, without excessively low or brightened enhanced images, ensuring visual quality in accordance with human perception.

4.2 Exposure Correction Experiments

Secondly, we conducted experiments in exposure correction task to further verify our method’s effectiveness. Here we choose **ME** dataset [5] which contains 24,330 8-bit sRGB images, and divided into 17,675 training images, 750 validation images, and 5905 test images. **ME** dataset is rendered from MIT-Adobe FiveK [5] dataset’s RAW data with 5 different exposure values (EVs), where EVs ranging from $\{-1.5, -1, 0, +1, +1.5\}$, including under-exposure to over-exposure conditions. This task aims to assess the model’s capability to simultaneously adjust both under & over-exposure conditions.

We show the experimental results in Table. 2, we compare **IAC** with various methods, including traditional methods histogram equalization (HE) [13] and LIME [15], SOTA deep-network based image enhancement methods [14, 30, 39, 40] and SOTA deep-network based

Table 2: Comparison results on the exposure correction ME [8] dataset, where the best results are marked as bold and second best results are marked as underline.

Method	Expert A		Expert B		Expert C		Expert D		Expert E		Avg		Test Time ↓
	PSNR↑	SSIM↑	PSNR↑	SSIM↑	PSNR↑	SSIM↑	PSNR↑	SSIM↑	PSNR↑	SSIM↑	PSNR↑	SSIM↑	
HE [10]	16.14	0.685	16.28	0.671	16.52	0.696	16.63	0.668	17.30	0.688	16.58	0.682	0.50s
LIME [11]	11.15	0.590	11.83	0.610	11.52	0.607	12.64	0.628	13.61	0.653	12.15	0.618	10.32s
RetinexNet [12]	10.76	0.585	11.61	0.596	11.13	0.605	11.99	0.615	12.67	0.636	11.63	0.607	1.08s
Deep-UPE [13]	13.16	0.610	13.90	0.642	13.69	0.632	14.80	0.649	15.68	0.667	14.25	0.640	0.78s
Zero-DCE [14]	11.64	0.536	12.56	0.539	12.06	0.544	12.96	0.548	13.77	0.580	12.60	0.549	0.04s
3D-LUT [15]	13.68	0.591	11.86	0.577	12.79	0.627	12.96	0.548	14.51	0.602	13.06	0.519	0.28s
SCI [16]	16.11	0.737	17.15	0.805	16.36	0.764	16.51	0.766	16.09	0.761	16.44	0.767	0.17s
MSEC [9]	19.16	0.746	20.10	0.734	20.20	0.769	18.98	0.719	18.98	0.727	19.48	0.739	0.72s
IAT [9]	<u>19.63</u>	<u>0.780</u>	21.21	<u>0.816</u>	21.21	<u>0.820</u>	19.58	<u>0.805</u>	19.21	<u>0.797</u>	20.07	<u>0.804</u>	0.11s
PSENet [17]	19.90	0.817	21.65	0.867	21.23	0.850	19.86	0.844	19.34	0.840	20.34	0.844	0.28s
MSLT [18]	20.21	0.805	22.47	0.864	<u>22.03</u>	0.844	20.33	0.830	<u>20.04</u>	0.832	<u>21.02</u>	0.835	0.24s
IAC (Ours)	21.23	0.829	<u>21.84</u>	0.870	22.05	0.859	<u>20.09</u>	0.846	20.88	0.848	21.22	0.850	<u>0.09s</u>

exposure correction methods [9, 10, 14, 18]. From Table. 2 we can see that our method gain best performance in overall PSNR and SSIM, meanwhile keep a fast inference speed. We also show the visulization results in Fig. 6, our IAC demonstrates the capability to effectively correct overexposure and enhance underexposure, while also efficiently preserving image details. An example in underexposure "Night" scene (Fig. 6 line 1~2) shows that, Zero-DCE [14], MSEC [9], and PSENet [17] tend to over-brighten images, potentially causing them to lose details, meanwhile IAT [9] and MSLT [18] may result in low clarity.

4.3 White Balance Editing Experiments

For white balance editing task, we utilize the Rendered WB dataset created by Afifi *et al.* [20], this dataset comprises two subsets: **Set1**, containing 62,535 images captured by seven distinct DSLR cameras, and **Set2**, containing 2,881 images captured by one DSLR camera and four different phone cameras. Here we follow previous works' [20, 21] setting, which take **Set1** for training and use **Set2** for testing, same as previous work [20], we randomly choose 12,000 images in **Set1** as the training set.

We made comparison with various WB editing methods, including the classical White Patch [22] method, along with recent methods FC4 [23], KNN-WB [24] and CNN-WB [25]. Comparison results are shown in Table. 3, we can see IAC can achieve competitive results meanwhile keep fastest inference speed. Additionally our method is much more light-weight than CNN-WB [25] (IAC $\sim 39.7K$ v.s. CNN-WB $\sim 10M$), some visualization results in Set2 are shown in Fig. 5, demonstrates that IAC could also handle white balance editing task.

5 Conclusion

We present IAC, which learns an image-adaptive coordinate system for various photography processing tasks. Experimental results on photo retouching, exposure correction, and white balance editing showcase the superior performance of our method. In the future, we aim to extend the coordinate transformation solution to curved surface, our algorithm may yield

Table 3: Comparison results on the white balance editing dataset [10]’s Set2, yellow colour shows best results and blue colour shows second best results.

Methods	MSE ↓				MAE ↓				Delta E 2000 ↓				Inference Time
	Mean	Q1	Q2	Q3	Mean	Q1	Q2	Q3	Mean	Q1	Q2	Q3	
White Patch	586.72	148.65	335.76	664.41	11.26	6.28	10.17	16.89	12.28	8.79	12.07	15.01	0.15s
FC4	505.30	142.46	307.77	635.35	10.37	5.94	9.42	14.04	10.82	7.39	10.64	13.77	0.89s
KNN-WB	171.09	37.04	87.04	190.88	4.48	2.26	3.64	5.95	5.60	3.43	4.90	7.06	0.54s
CNN-WB	124.97	30.13	76.32	154.44	3.75	2.02	3.08	4.72	4.90	3.13	4.35	6.08	1.2s
Ours	130.58	33.22	72.56	180.48	3.99	1.98	3.44	4.87	5.13	3.24	4.48	6.27	0.05s

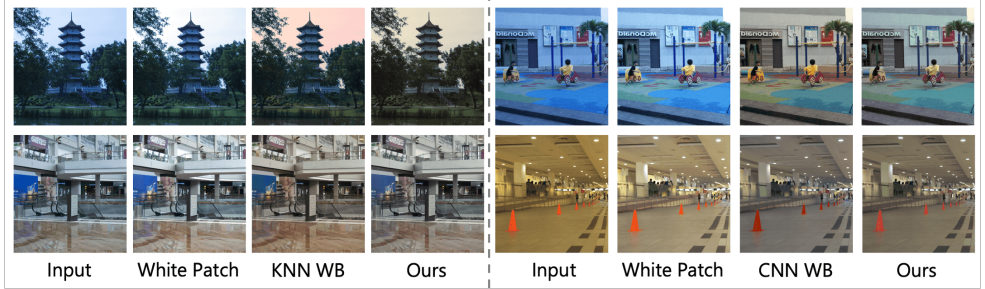


Figure 5: Visualization of white balance editing results on dataset [10]’s Set2.

even better results in non-uniform coordinate spaces, we also want validate the effectiveness of IAC for 3D application, such as 3D reconstruction in challenging lighting conditions [11].

6 Acknowledgement

This work was partially supported by JST Moonshot R&D Grant Number JPMJPS2011, CREST Grant Number JPMJCR2015 and Basic Research Grant (Super AI) of Institute for AI and Beyond of the University of Tokyo.

References

- [1] Mahmoud Afifi and Michael S. Brown. Deep white-balance editing. In *Proceedings of the IEEE/CVF Conference on Computer Vision and Pattern Recognition (CVPR)*, June 2020.
- [2] Mahmoud Afifi, Brian Price, Scott Cohen, and Michael S Brown. When color constancy goes wrong: Correcting improperly white-balanced images. In *Proceedings of the IEEE Conference on Computer Vision and Pattern Recognition*, pages 1535–1544, 2019.
- [3] Mahmoud Afifi, Konstantinos G Derpanis, Bjorn Ommer, and Michael S Brown. Learning multi-scale photo exposure correction. In *Proceedings of the IEEE/CVF Conference on Computer Vision and Pattern Recognition*, pages 9157–9167, 2021.
- [4] David H Brainard and Brian A Wandell. Analysis of the retinex theory of color vision. *JOSA A*, 3(10):1651–1661, 1986.

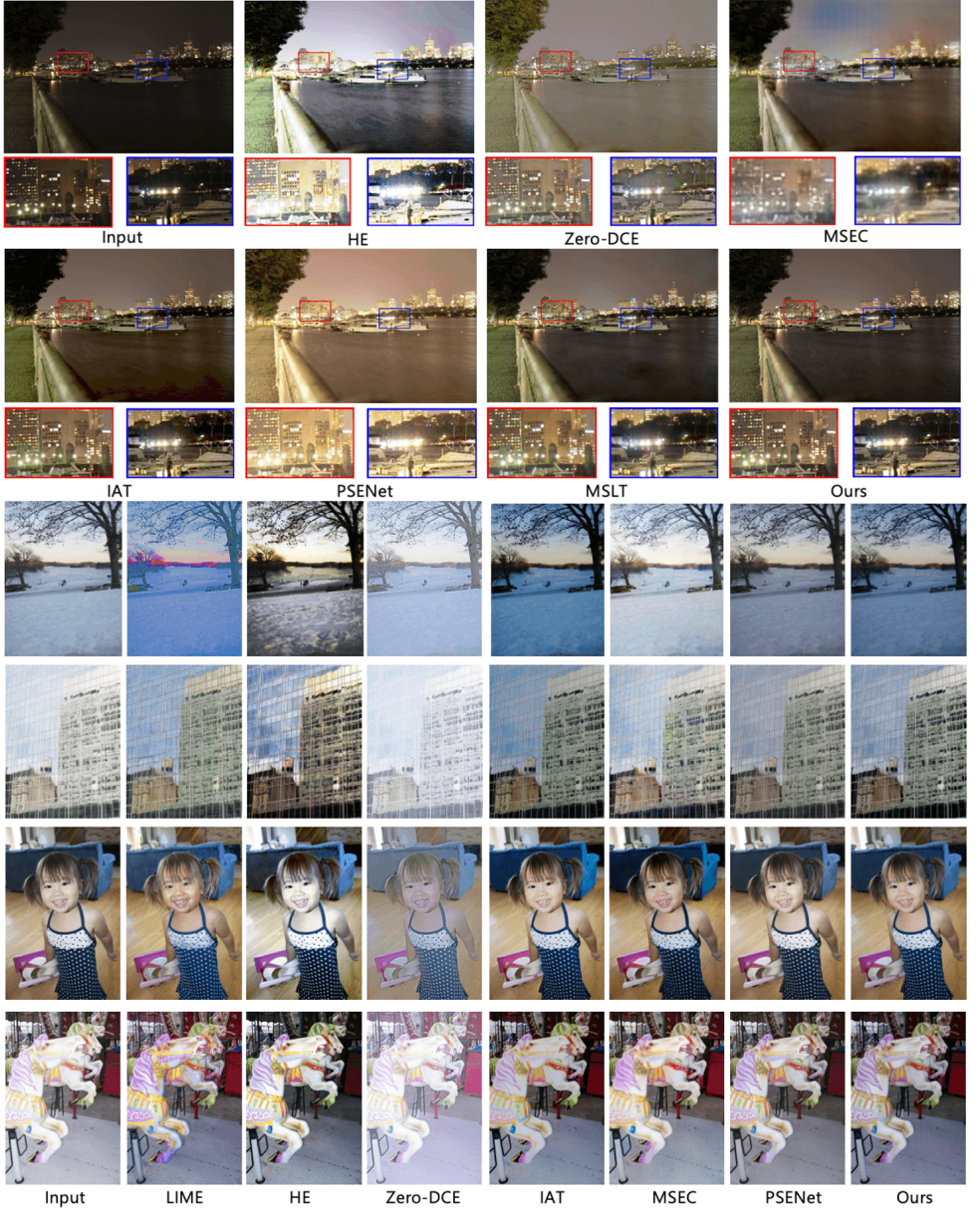


Figure 6: Visualization results on exposure correction dataset [9], line 1 and line 2 are the under-exposure correction results, meanwhile line 3 to line 6 are the over-exposure correction results, our method could both handle over&under-exposure meanwhile keep more details.

- [5] Vladimir Bychkovsky, Sylvain Paris, Eric Chan, and Frédo Durand. Learning photographic global tonal adjustment with a database of input / output image pairs. In *Proceedings of the IEEE Conference on Computer Vision and Pattern Recognition*, 2011.
- [6] Yuanhao Cai, Hao Bian, Jing Lin, Haoqian Wang, Radu Timofte, and Yulun Zhang. Retinexformer: One-stage retinex-based transformer for low-light image enhancement. In *Proceedings of the IEEE/CVF International Conference on Computer Vision (ICCV)*, pages 12504–12513, October 2023.
- [7] Yu-Sheng Chen, Yu-Ching Wang, Man-Hsin Kao, and Yung-Yu Chuang. Deep photo enhancer: Unpaired learning for image enhancement from photographs with gans. In *IEEE/CVF Conference on Computer Vision and Pattern Recognition*, 2018.
- [8] Marcos V Conde, Javier Vazquez-Corral, Michael S Brown, and Radu Timofte. Nilut: Conditional neural implicit 3d lookup tables for image enhancement. In *Proceedings of the AAAI Conference on Artificial Intelligence*, 2024.
- [9] Ziteng Cui, Kunchang Li, Lin Gu, Shenghan Su, Peng Gao, ZhengKai Jiang, Yu Qiao, and Tatsuya Harada. You only need 90k parameters to adapt light: a light weight transformer for image enhancement and exposure correction. In *33rd British Machine Vision Conference 2022, BMVC 2022, London, UK, November 21-24, 2022*. BMVA Press, 2022. URL <https://bmvc2022.mpi-inf.mpg.de/0238.pdf>.
- [10] Ziteng Cui, Lin Gu, Xiao Sun, Xianzheng Ma, Yu Qiao, and Tatsuya Harada. Alethnerf: Illumination adaptive nerf with concealing field assumption. In *Proceedings of the AAAI Conference on Artificial Intelligence*, 2024.
- [11] Mauricio Delbracio, Damien Kelly, Michael S. Brown, and Peyman Milanfar. Mobile computational photography: A tour. *Annual Review of Vision Science*, 7(1):571–604, 2021. doi: 10.1146/annurev-vision-093019-115521. URL <https://doi.org/10.1146/annurev-vision-093019-115521>. PMID: 34524880.
- [12] Michaël Gharbi, Jiawen Chen, Jonathan T Barron, Samuel W Hasinoff, and Frédo Durand. Deep bilateral learning for real-time image enhancement. *ACM Transactions on Graphics (TOG)*, 36(4):1–12, 2017.
- [13] Rafael C. Gonzalez and Richard E. Woods. *Digital Image Processing (3rd Edition)*. Prentice-Hall, Inc., USA, 2006. ISBN 013168728X.
- [14] C. Guo, C. Li, J. Guo, C. C. Loy, J. Hou, S. Kwong, and R. Cong. Zero-reference deep curve estimation for low-light image enhancement. In *IEEE/CVF Conference on Computer Vision and Pattern Recognition*, 2020.
- [15] Xiaojie Guo, Yu Li, and Haibin Ling. Lime: Low-light image enhancement via illumination map estimation. *IEEE Transactions on Image Processing*, 2017.
- [16] Trevor Hastie, Robert Tibshirani, Jerome H Friedman, and Jerome H Friedman. *The elements of statistical learning: data mining, inference, and prediction*, volume 2. Springer, 2009.

- [17] Dan Hendrycks and Kevin Gimpel. Bridging nonlinearities and stochastic regularizers with gaussian error linear units. *CoRR*, abs/1606.08415, 2016. URL <http://arxiv.org/abs/1606.08415>.
- [18] Yuanming Hu, Baoyuan Wang, and Stephen Lin. Fc 4: Fully convolutional color constancy with confidence-weighted pooling. In *Proceedings of the IEEE Conference on Computer Vision and Pattern Recognition*, pages 4085–4094, 2017.
- [19] Andrey Ignatov, Nikolay Kobyshev, Radu Timofte, Kenneth Vanhoey, and Luc Van Gool. Dslr-quality photos on mobile devices with deep convolutional networks. In *Proceedings of the IEEE international conference on computer vision*, 2017.
- [20] Ting Jiang, Chuan Wang, Xinpeng Li, Ru Li, Haoqiang Fan, and Shuaicheng Liu. Meflut: Unsupervised 1d lookup tables for multi-exposure image fusion. In *Proceedings of the IEEE/CVF International Conference on Computer Vision*, pages 10542–10551, 2023.
- [21] Justin Johnson, Alexandre Alahi, and Li Fei-Fei. Perceptual losses for real-time style transfer and super-resolution. In *European Conference on Computer Vision*, 2016.
- [22] Bomi Kim, Sunhyeok Lee, Nahyun Kim, Donggon Jang, and Dae-Shik Kim. Learning color representations for low-light image enhancement. In *2022 IEEE/CVF Winter Conference on Applications of Computer Vision (WACV)*, pages 904–912, 2022. doi: 10.1109/WACV51458.2022.00098.
- [23] Han-UI Kim, Young Jun Koh, and Chang-Su Kim. Global and local enhancement networks for paired and unpaired image enhancement. In Andrea Vedaldi, Horst Bischof, Thomas Brox, and Jan-Michael Frahm, editors, *Computer Vision – ECCV 2020*, pages 339–354, Cham, 2020. Springer International Publishing. ISBN 978-3-030-58595-2.
- [24] Hanul Kim, Su-Min Choi, Chang-Su Kim, and Yeong Jun Koh. Representative colour transform for image enhancement. In *Proceedings of the IEEE/CVF International Conference on Computer Vision*, 2021.
- [25] Furkan Kinli, Dogacan Yilmaz, Barış Özcan, and Mustafa Furkan Kırac. Modeling the lighting in scenes as style for auto white-balance correction. *2023 IEEE/CVF Winter Conference on Applications of Computer Vision (WACV)*, pages 4892–4902, 2022. URL <https://api.semanticscholar.org/CorpusID:252917913>.
- [26] Furkan Kinli, Dogacan Yilmaz, Barış Özcan, and Mustafa Furkan Kırac. Deterministic neural illumination mapping for efficient auto-white balance correction. *2023 IEEE/CVF International Conference on Computer Vision Workshops (ICCVW)*, pages 1131–1139, 2023. URL <https://api.semanticscholar.org/CorpusID:260704581>.
- [27] Gehui Li, Jinyuan Liu, Long Ma, Zhiying Jiang, Xin Fan, and Risheng Liu. Fearless luminance adaptation: A macro-micro-hierarchical transformer for exposure correction. In *Proceedings of the 31st ACM International Conference on Multimedia*, MM ’23, page 7304–7313, New York, NY, USA, 2023. Association for Computing Machinery. ISBN 9798400701085.

- [28] Chengxu Liu, Huan Yang, Jianlong Fu, and Xueming Qian. 4d lut: learnable context-aware 4d lookup table for image enhancement. *IEEE Transactions on Image Processing*, 32:4742–4756, 2023.
- [29] Zhuang Liu, Hanzi Mao, Chao-Yuan Wu, Christoph Feichtenhofer, Trevor Darrell, and Saining Xie. A convnet for the 2020s. *Proceedings of the IEEE/CVF Conference on Computer Vision and Pattern Recognition (CVPR)*, 2022.
- [30] Long Ma, Tengyu Ma, Risheng Liu, Xin Fan, and Zhongxuan Luo. Toward fast, flexible, and robust low-light image enhancement. In *Proceedings of the IEEE/CVF Conference on Computer Vision and Pattern Recognition*, pages 5637–5646, 2022.
- [31] Sean Moran, Pierre Marza, Steven McDonagh, Sarah Parisot, and Gregory Slabaugh. Deeplpf: Deep local parametric filters for image enhancement. In *Proceedings of the IEEE/CVF Conference on Computer Vision and Pattern Recognition*, 2020.
- [32] Sean Moran, Steven McDonagh, and Gregory Slabaugh. Curl: Neural curve layers for global image enhancement. In *2020 25th International Conference on Pattern Recognition (ICPR)*, pages 9796–9803, 2021. doi: 10.1109/ICPR48806.2021.9412677.
- [33] Nayar and Branzoi. Adaptive dynamic range imaging: optical control of pixel exposures over space and time. In *Proceedings Ninth IEEE International Conference on Computer Vision*, pages 1168–1175 vol.2, 2003. doi: 10.1109/ICCV.2003.1238624.
- [34] Hue Nguyen, Diep Tran, Khoi Nguyen, and Rang Nguyen. Psenet: Progressive self-enhancement network for unsupervised extreme-light image enhancement. In *Proceedings of the IEEE/CVF Winter Conference on Applications of Computer Vision*, pages 1756–1765, 2023.
- [35] Zhaolin Qiu, Jiaqing Liu, Hao Sun, Lanfen Lin, and Yen-Wei Chen. Costhr: A heart rate estimating network with adaptive color space transformation. *IEEE Transactions on Instrumentation and Measurement*, 71:1–10, 2022. doi: 10.1109/TIM.2022.3170976.
- [36] Carl Edward Rasmussen. *Gaussian Processes in Machine Learning*, pages 63–71. Springer Berlin Heidelberg, Berlin, Heidelberg, 2004. ISBN 978-3-540-28650-9. doi: 10.1007/978-3-540-28650-9_4. URL https://doi.org/10.1007/978-3-540-28650-9_4.
- [37] Yuda Song, Hui Qian, and Xin Du. Starenhancer: Learning real-time and style-aware image enhancement. In *Proceedings of the IEEE/CVF International Conference on Computer Vision*, pages 4126–4135, 2021.
- [38] Yael Vinker, Inbar Huberman-Spiegelglas, and Raanan Fattal. Unpaired learning for high dynamic range image tone mapping. In *Proceedings of the IEEE/CVF international conference on computer vision*, pages 14657–14666, 2021.
- [39] Ruixing Wang, Qing Zhang, Chi-Wing Fu, Xiaoyong Shen, Wei-Shi Zheng, and Jiaya Jia. Underexposed photo enhancement using deep illumination estimation. In *The IEEE Conference on Computer Vision and Pattern Recognition*, 2019.

- [40] Tao Wang, Yong Li, Jingyang Peng, Yipeng Ma, Xian Wang, Fenglong Song, and Youliang Yan. Real-time image enhancer via learnable spatial-aware 3d lookup tables. In *Proceedings of the IEEE/CVF International Conference on Computer Vision*, pages 2471–2480, 2021.
- [41] Chen Wei, Wenjing Wang, Wenhan Yang, and Jiaying Liu. Deep retinex decomposition for low-light enhancement. In *British Machine Vision Conference*, 2018.
- [42] Canqian Yang, Meiguang Jin, Xu Jia, Yi Xu, and Ying Chen. Adaint: Learning adaptive intervals for 3d lookup tables on real-time image enhancement. In *Proceedings of the IEEE/CVF Conference on Computer Vision and Pattern Recognition (CVPR)*, 2022.
- [43] Shuzhou Yang, Moxuan Ding, Yanmin Wu, Zihan Li, and Jian Zhang. Implicit neural representation for cooperative low-light image enhancement. In *Proceedings of the IEEE/CVF International Conference on Computer Vision (ICCV)*, pages 12918–12927, October 2023.
- [44] Shuzhou Yang, Xuanyu Zhang, Yinhuai Wang, Jiwen Yu, Yuhan Wang, and Jian Zhang. Diffle: Diffusion-guided domain calibration for unsupervised low-light image enhancement, 2023.
- [45] Lu Yuan and Jian Sun. Automatic exposure correction of consumer photographs. In *European Conference on Computer Vision*, 2012.
- [46] Hui Zeng, Jianrui Cai, Lida Li, Zisheng Cao, and Lei Zhang. Learning image-adaptive 3d lookup tables for high performance photo enhancement in real-time. *IEEE Transactions on Pattern Analysis and Machine Intelligence*, 44(04):2058–2073, 2022.
- [47] Fengyi Zhang, Lin Zhang, Tianjun Zhang, and Dongqing Wang. Adaptively hashing 3dluts for lightweight real-time image enhancement. In *2023 IEEE International Conference on Multimedia and Expo (ICME)*, pages 2771–2776, 2023. doi: 10.1109/ICME55011.2023.00471.
- [48] Yijie Zhou, Chao Li, Jin Liang, Tianyi Xu, Xin Liu, and Jun Xu. 4k-resolution photo exposure correction at 125 fps with 8k parameters. In *Winter Conference on Applications of Computer Vision (WACV)*, 2024.

A Experiments Setting

All experiments for **IAC** model on the 3 tasks (Photo Retouching, Exposure Correction, and White Balance Editing) were conducted on a single Nvidia A100 GPU. Next, we will provide a detailed explanation of the experimental settings and training details for each task.

A.1 Photo Retouching Setting

The MIT-Adobe FiveK [5] dataset contains 5,000 images, of which 4,500 are used for training and the remaining 500 for evaluation. The training images are uniformly resized to 400×600 and augmented with random flip and rotation. The training process uses the Adam optimizer with an initial learning rate of $1e^{-5}$ and a weight decay set to 0.0002. The model is trained for a total of 100 iterations, accompanied by a cosine annealing learning strategy.

The loss function between predicted image $F^{-1}(L(F(x)))$ and ground truth image \hat{x} is a mixed loss function \mathcal{L}_{mix} consisting of smooth L1 loss and VGG loss [24]:

$$\mathcal{L}_{mix} = \mathcal{L}_{smooth} + 0.04 \cdot \mathcal{L}_{vgg}. \quad (5)$$

A.2 Exposure Correction Setting

The exposure correction **ME** dataset [9] contains 24,330 images, which divided into 17,675 training images, 750 validation images, and 5905 test images. For the exposure correction task, the training images are cropped into 256×256 patches and augmented with random flip and rotation. We also adopt Adam optimizer same as photo retouching task, with an initial learning rate of $2e^{-5}$ and a weight decay set to 0.0001. The model is trained for a total of 20 iterations, also accompanied by a cosine annealing learning strategy. And the loss function we used in exposure correction task is L1 loss function.

A.3 White Balance Editing Setting

The White Balance Editing dataset [2], Rendered WB, includes two sets: **Set1** containing 62,535 images and **Set2** containing 2,881 images. We use 12,000 images from **Set1** for training. The training settings are the same as for the exposure correction tasks, except the number of training epochs is set to 100. We also adopt the L1 loss function for this task.

B Ablation Analyse

B.1 Curve Dimension Ablation

We conducted an ablation analysis on the dimensionality of curves on the exposure correction **ME** [9] dataset, investigating the impact of the dimensions of $\{curve_1, curve_2, curve_3\}$ on the experimental results. The experimental results are shown in Table. IV, from which we can observe that setting the dimension to 200 is a rather reasonable choice. Meanwhile, as shown in Fig. VII, setting a lower dimension easily leads to pixelation in the images.

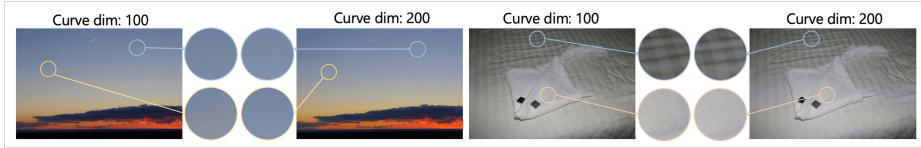


Figure VII: The ablation analyse of the curve dim’s effect.

Table IV: Ablation analyse on the curve dimension.

	dims 50	dims 100	dims 150	dims 200	dims 250
PSNR	17.67	20.45	20.88	21.22	21.24
SSIM	0.634	0.795	0.832	0.850	0.849

B.2 Network Structure Ablation

In our default experiments, we set the dimension size in ConvNext [29] block to 32, in the ablation study on photo retouching dataset [5], we attempted other dimension numbers such as 16, 24, and 64, as shown in Table. V. From the perspective of parameter count/FLOPs and overall performance, we found that setting it to 24 or 32 is a more reasonable choice. Furthermore, in the original network, we attempted to use three parallel branches to learn three sets of coordinates and their corresponding curves. Here, we also tried putting the three sets of coordinates and curves into a single branch for learning. However, we found that this approach led to a significant decrease in performance, as shown in Table. V (“unified branch”).

Table V: Ablation analyse on the ConvNext [29] block convolution dimension.

	size 16	size 24	size 32	size 64	unified branch (size 32)
PSNR	24.01	24.81	25.02	25.01	24.12
SSIM	0.872	0.897	0.902	0.895	0.865
parameters	16.7K	28.9K	39.7K	97.8K	25.4K
Flops	0.72 G	1.98 G	3.25 G	7.89 G	3.04 G